ORIGINAL PAPER

Magnetocaloric Effects in $Pr_{0.6-x}Er_xSr_{0.4}MnO_3$ ($0.0 \leq x \leq 0.2$) Manganese Oxides

**R. M'nassri · W. Cheikhrouhou-Koubaa · N. Boudjada ·
A. Cheikhrouhou**

Abstract The effects of partial substitution of praseodymium by erbium on the structural, magnetic, and magnetocaloric properties of $Pr_{0.6-x}Er_xSr_{0.4}MnO_3$ ($0.0 \leq x \leq 0.2$) powder samples have been studied. Our polycrystalline compounds were synthesized by the conventional solid state reaction at high temperature. Rietveld refinement of the X-ray diffraction patterns using Fullprof program shows that all our samples are single phase and crystallize in the orthorhombic structure with the *Pnma* space group. The unit cell volume decreased with increasing the Er amount. Magnetic measurements show that all our samples exhibit a paramagnetic–ferromagnetic transition with decreasing temperature. The Curie temperature T_C shifts to lower values with increasing Er content. From the magnetization isotherms at different temperatures, magnetic entropy changes ΔS_M and relative cooling power RCP have been evaluated. The maximum of the magnetic entropy changes for the $Pr_{0.45}Er_{0.15}Sr_{0.4}MnO_3$ sample is found to be $|\Delta S_M^{\max}| = 2.66 \, \text{J kg}^{-1} \text{K}^{-1}$ under a magnetic applied field change of 2 T.

Keywords Manganites · Magnetization · Magnetocaloric effect · Relative cooling power

R. M'nassri (✉) · W. Cheikhrouhou-Koubaa · A. Cheikhrouhou
Laboratoire de Physique des Matériaux, Faculté des Sciences de Sfax, Sfax University, B.P. 1171, 3000 Sfax, Tunisia
e-mail: abdcheikhrouhou@yahoo.fr

R. M'nassri · N. Boudjada · A. Cheikhrouhou
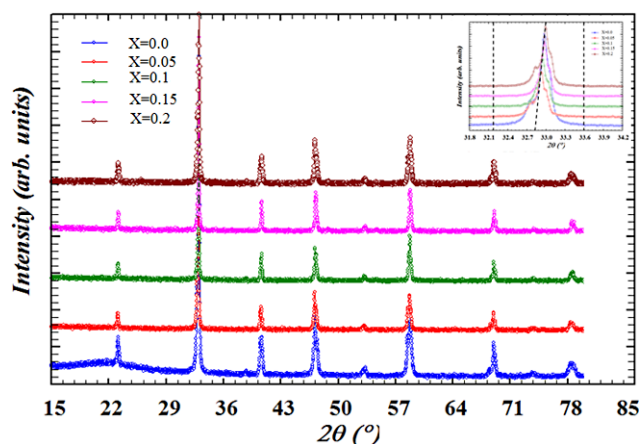Institut NEEL, B.P. 166, 38042 Grenoble Cedex 9, France

1 Introduction

During the last 15 years, the mixed valent manganites with perovskite structure $Ln_{1-x}M_xMnO_3$ (Ln = rare-earth element and M = divalent metal such as Ca, Sr, Ba, etc.) have been the subject of very important research due to their magnetic, colossal magnetoresistance, and recently the magnetocaloric effect that they exhibit [1] along with their great potential for use in a wide range of applications including sensors and magnetic refrigeration technology. The perovskite structure shows generally lattice distortion as modifications from the cubic structure to rhombohedral or orthorhombic one mainly due to the Jahn–Teller (JT) effect distortion [2]. The double exchange theory and the Jahn–Teller effect were used to understand the ferromagnetic–paramagnetic phase transition associated to the insulator–metal one in these materials [3, 4], thus giving rise to the well-known colossal magnetoresistance (CMR) [1].

The perovskite manganite $Pr_{1-x}Sr_xMnO_3$ is an important member of the manganite family with intermediate one electron bandwidth [5]. The Pr-based manganites show several properties including charge ordering state, ferromagnetic, and antiferromagnetic coexistence, and metamagnetic transition [6–9]. For $x < 0.5$, it possesses a strong ferromagnetic–paramagnetic transition with decreasing temperature, a large magnetoresistance in the vicinity of T_C, and an important magentocaloric effect (MCE). In order to continue our search for new magnetocaloric materials with possibility to be used in magnetic refrigeration around room temperature, we report in this paper the effect of Er doping on the magnetic and magnetocaloric proprieties of $Pr_{0.6}Sr_{0.4}MnO_3$. The T_C of the parent compound is found to be 310 K [10].

**Fig. 1** XRD patterns at room temperature of $Pr_{0.6-x}Er_xSr_{0.4}MnO_3$ ($0.0 \leq x \leq 0.2$). *Inset*: a zoom on the main peak

2 Experimental Techniques

Polycrystalline $Pr_{0.6-x}Er_xSr_{0.4}MnO_3$ ($0.0 \leq x \leq 0.2$) samples were prepared using the conventional solid-state reaction method at high temperatures. Stoichiometric powders of Pr_6O_{11}, $SrCO_3$, Er_2O_3, and MnO_2 were mixed with the desired proportions according to the reaction:

$$(0.6 - x)Pr_6O_{11} + 3xEr_2O_3 + 2.4SrCO_3 + 6MnO_2$$
$$\rightarrow 6Pr_{0.6-x}Er_xSr_{0.4}MnO_3 + \delta CO_2 + \delta'O_2$$
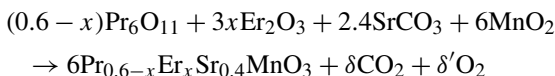
The starting materials, ground in an agate mortar and pressed into pellets, were heated in air at 1000 °C and 1250 °C for 60 h with intermediate grinding. The obtained powders were pressed into pellets and sintered at 1350 °C in air for 60 h with intermediate regrinding and repelling. Finally, these pellets were cooled slowly to room temperature in air. The physical properties depend strongly on the synthesis route and also on the cooling method. Phase purity, homogeneity, and cell dimensions were determined by X-ray powder diffraction (XRD) at room temperature (diffractometer using Cu Kα radiation). Structural analysis was carried out using the standard Rietveld method [11, 12]. Magnetizations (M) versus temperature (T) and versus magnetic applied field (H) were measured using a vibrating sample magnetometer equipped with a superconducting coil. $M(T)$ data were obtained under 0.05 T in the temperature range 20–300 K in the field cooled mode, while $M(H)$ data up to 7 T were recorded at several temperatures in the range 20–350 K.

3 Results and Discussion

We report in Fig. 1 the XRD patterns at room temperature of all our synthesized samples. A zoom on the main peak shows a shift to high angles indicating a decrease of the unit cell
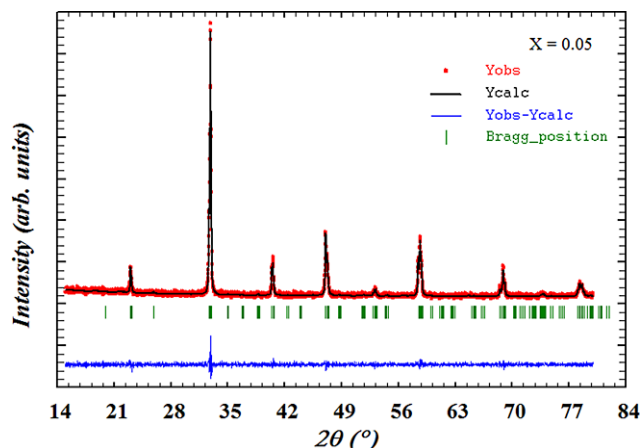
(a)
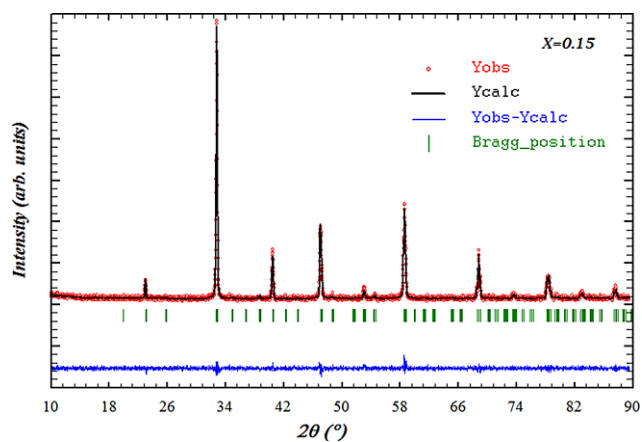
(b)

Fig. 2 Observed (*solid circles*) and calculated (*solid line*) XRD patterns of the Er-doped samples ($x = 0.05$ and $x = 0.15$) at room temperature. The difference between these spectra is plotted at the *bottom*. Bragg reflections are indicated by *ticks*

volume. All our samples were found to be single phase and have the same perovskite structure. Figure 2 shows typical XRD patterns registered at room temperature for $x = 0.05$ and 0.15 samples. The data were refined by the Rietveld technique using the Fullprof program. XRD patterns can be indexed in the orthorhombic system with Pnma space group for all samples. The quality of the refinement is evaluated through the goodness of the fit indicator χ^2. The structural parameters are listed in Table 1.

With increasing Er content, the unit cell volume of our samples decreases monotonously from 229.36 for $x = 0.0$ to 227.56 for $x = 0.2$ (see Fig. 3). This behavior can be explained in terms of average ionic radius values of the A-site; in fact, the average ionic radius of Er^{3+} (1.062 Å) is smaller than that of Pr^{3+} (1.179 Å) [13, 14]. The cationic disorder as well as the distortion of the MnO_6 octahedral due to the erbium doping may also explain our results [15, 16].

Fig. 3 The unit cell volume and T_C versus x for $Pr_{0.6-x}Er_xSr_{0.4}MnO_3$ ($0.0 \leq x \leq 0.2$)

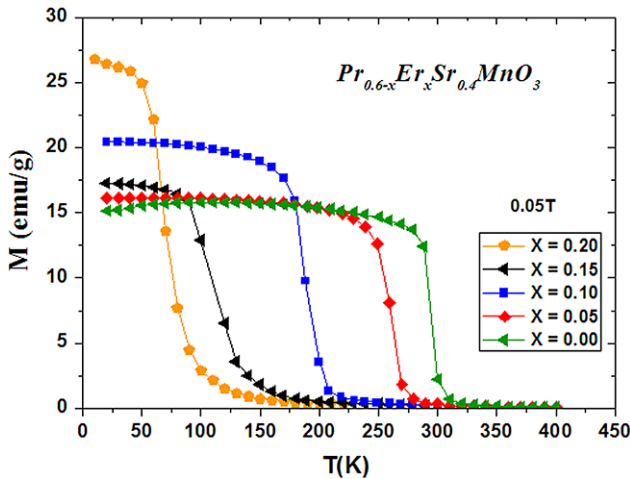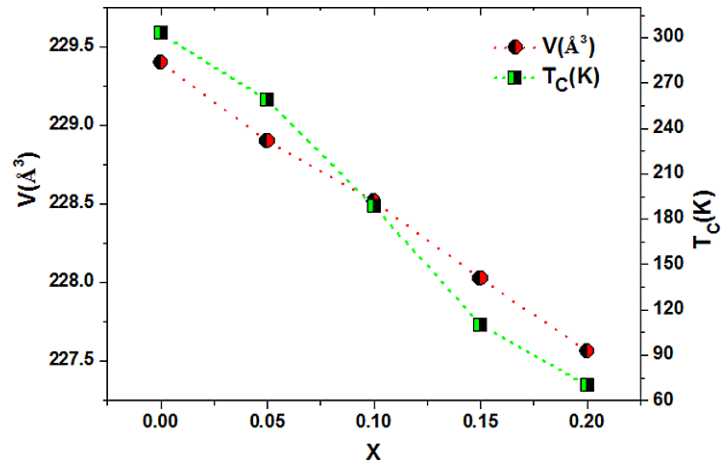**Fig. 4** Magnetization measurements as a function of temperature for $Pr_{0.6-x}Er_xSr_{0.4}MnO_3$ ($0.0 \leq x \leq 0.2$) samples under 0.05 T

Table 1 Refined structural parameters of $Pr_{0.6-x}Er_xSr_{0.4}MnO_3$ ($0.0 \leq x \leq 0.2$) compounds at room temperature

Parameter	$x = 0.0$	$x = 0.05$	$x = 0.1$	$x = 0.15$	$x = 0.2$
a (Å)	5.4445	5.4438	5.4442	5.4439	5.4415
b (Å)	7.6801	7.6838	7.6846	7.6825	7.6744
c (Å)	5.4854	5.4723	5.4621	5.4523	5.4493
V (Å³)	229.36	228.90	228.51	228.02	227.56
Mn–O$_1$–Mn (°)	160.86	163.52	162.14	164.84	160.4716
Mn–O$_2$–Mn (°)	162.513	161.719	161.2	162.2	161.614
Mn–O$_1$ (Å)	1.9475	1.9416	1.94510	1.9389	1.9504
Mn–O$_{2\text{-I}}$ (Å)	2.003	1.994	2.055	2.045	1.983
Mn–O$_{2\text{-II}}$ (Å)	1.913	1.925	1.865	1.865	1.933
χ^2	1.19	1.20	1.24	1.17	1.21

4 Magnetic Properties

Figure 4 shows the temperature dependence of the magnetization M at a magnetic applied field of 0.05 T in the

field-cooled (FC) mode for our samples. We observe a sharp transition from high-temperature paramagnetic state to low-temperature ferromagnetic state. The $M(T)$ curves do not reveal secondary magnetic phases, which confirm the good crystallization of our samples. As shown in Fig. 3, the Curie temperature T_C, which is defined as the inflection point of $M(T)$ curve, decreases drastically from 303 K ($x = 0.0$) to 70 K ($x = 0.2$) with increasing Er-content. This is direct evidence of the effective reduction of the interaction between the Mn ions and weakens the double-exchange. It is known that two parameters have been considered to be relevant concerning the electronic and magnetic properties of these compounds, namely, the amount of Mn^{4+} or the average manganese oxidation state (directly related to the concentration of carriers in the e_g orbitals) and the average ionic radius $\langle r_A \rangle$ of the A site. As the Mn^{4+} remains constant (Er^{3+} and Pr^{3+} have both the same valence), the second parameter $\langle r_A \rangle$ is responsible for the variation of T_C. It has been supposed that this effect is related to changes of the charge-carrier bandwidth W, which describes electron hopping from the Mn sites [17]. With increasing Er content, the mean size of the cations in the A site decreases and varies the symmetry of the crystal structure. As a result, the Mn–O bond length and Mn–O–Mn bond angle is adjusted, the ferromagnetic coupling is weakened and T_C drops [17, 18]. Our results are in concordance with Moutis et al. [19] and Wang et al. [20] reports: the Curie temperature decreases with decreasing the mean size of the cations in the Ln site, $\langle r_A \rangle$).

In order to confirm the ferromagnetic behavior at low temperatures, we have performed magnetization measurements as a function of the magnetic applied field $\mu_0 H$ up to 7 T at several temperatures. Figure 5 shows $M(H)$ curves for $x = 0.05$ and $x = 0.15$. The magnetization increases sharply with magnetic applied field for $H < 0.5$ T but does not reach saturations up to 7 T indicating that the magnetic moment of the rare-earth ions are polarized and pinned by the Mn-sublattice [21]. Therefore, the magnetization is weakly dependent on the magnetic applied field in the high
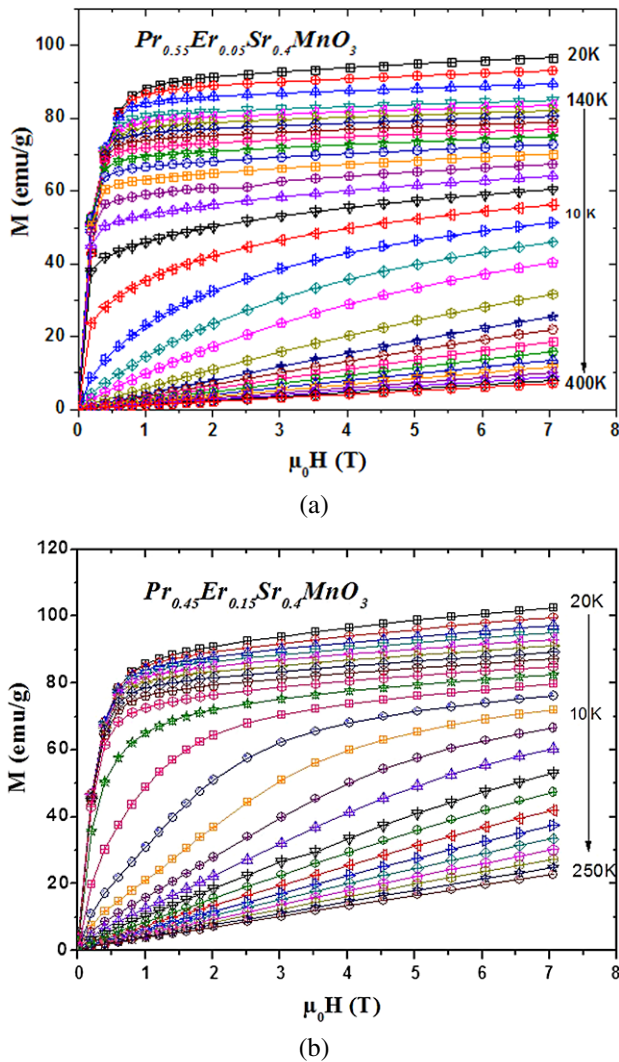
(a)

(b)

Fig. 5 Isothermal magnetization $M(H)$ for $Pr_{0.6-x}Er_xSr_{0.4}MnO_3$ samples measured at several temperatures: (**a**) $x = 0.1$ and (**b**) $x = 0.2$

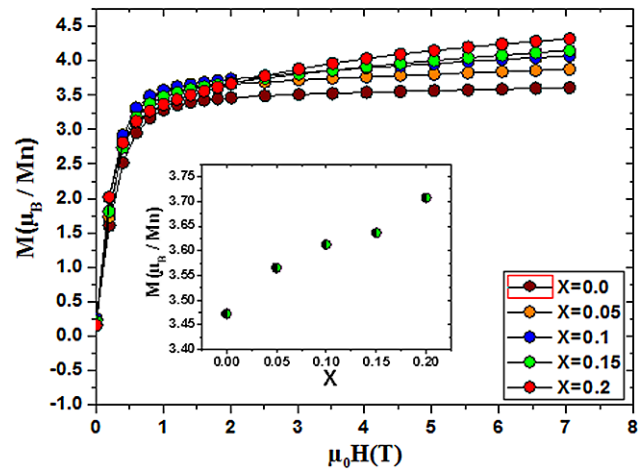**Fig. 6** Magnetization versus magnetic applied field at 20 K for $Pr_{0.6-x}Er_xSr_{0.4}MnO_3$ ($0.0 \leq x \leq 0.2$). The *inset* shows the evolution of M_{sp}(exp) versus x

field region. The high field dependence of the magnetization is enhanced with the increase of Er content. As it was previously highlighted, the Mn–Mn interaction strength is weakened by Er^{3+} doping. The paramagnetic moment of Er^{3+} ions at the A-site will interact with Mn^{3+} and Mn^{4+} ions at the B-site, which weakens the double exchange interaction and results in the decrease of T_C. The explanation is that the magnetic moments of Mn^{3+} ions are much smaller than the magnetic moments of Er^{3+} ions. Therefore, the magnetization does not reach the saturation for high field values. At 20 K, the magnetization keeps increasing with increasing magnetic field to quantities well above the value of the ordered moment of Mn^{3+} and Mn^{4+}. This result indicates that both ferromagnetism of the Mn ions and paramagnetism of the rare-earth ions contribute to the low temperature magnetization. We report in Fig. 6 the $M(H)$ curves at 20 K for $Pr_{0.6-x}Er_xSr_{0.4}MnO_3$ ($0.0 \leq x \leq 0.2$). The experimental values of the spontaneous magnetization, M_{sp}(exp), are

found to be 3.47 and 3.56 μ_B/Mn for $x = 0.0$ and 0.05, slightly lower than the theoretical value of 3.6 μ_B/Mn obtained for full spin alignment. For $x = 0.1$, 0.15, and 0.2, the M_{sp}(exp) are found to be 3.61 μ_B/Mn, 3.64 μ_B/Mn and 3.71 μ_B/Mn, respectively. These values are slightly higher than the theoretical one (see in the inset of Fig. 6). The significant increase of the magnetization indicates the magnetic ordering of rare earth ions in the manganites.

To characterize the first-order or second-order phase transition, the purely magnetic ways to determine are the Banerjee criteria in 1964 [22], by analyzing H/M versus M^2 curves. Banerjee [22] detected the essential similarity between the Landau–Lifshitz and the Bean–Rodbell criteria and condensed them into one that provides a tool to distinguish first-order from second-order magnetic transitions. It consists in the observation of the slope of isotherm plots of H/M versus M^2. In order to determine the order of the magnetic phase transition of both $Pr_{0.6-x}Er_xSr_{0.4}MnO_3$ ($x = 0.05$, 0.15, and 0.2) samples, Arrott plots (M^2 vs. H/M) are shown in Fig. 7. The transition is of first order when the slope of the isotherm M^2 vs. H/M is negative and of second order in the other case [23, 24]. Positive slope is observed in the Arrott plots of both $x = 0.05, 0.15$, and $x = 0.2$, which reflects the second-order phase transition. The T_C values deduced from the Arrott curves (T_C corresponds to the isotherm passing through the origin) [22, 25] are very close to that obtained from the $M(T)$ ones.

5 Magnetocaloric Effect

In an isothermal process of magnetization, the magnetocaloric effect (MCE) of the materials can be derived from the Maxwell's thermodynamic relationship [26]:
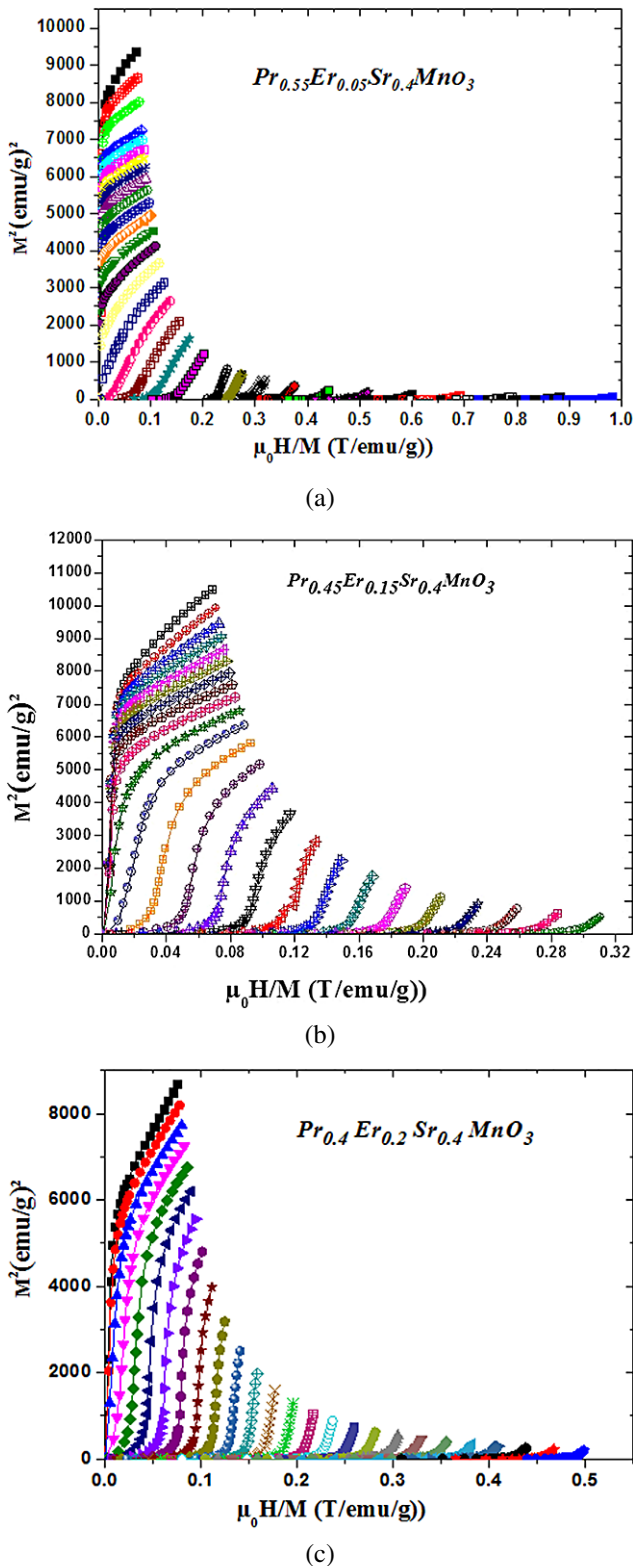
Fig. 7 Arrott curves M^2 versus $\mu_0 H/M$ for $Pr_{0.6-x}Er_xSr_{0.4}MnO_3$ sample: (**a**) $x = 0.1$ and (**b**) $x = 0.2$

$$\left(\frac{\partial M}{\partial T}\right)_H = \left(\frac{\partial S}{\partial H}\right)_T \tag{1}$$

the magnetic-entropy change ΔS_M, which results from the spin ordering (i.e. ferromagnetic ordering) and is induced by the variation of the magnetic applied field from 0 to H_{max} is given by

$$\Delta S_M(T, H_{max}) = S_M(T, H_{max}) - S_M(T, 0)$$
$$= \int_0^{H_{max}} \left(\frac{\partial M}{\partial T}\right)_H dH \tag{2}$$

For magnetization measured at discrete field and temperature intervals, the magnetic entropy change defined in Eq. (2) can be approximated by Eq. (3) [27],

$$\Delta S_M = \sum_i \frac{M_i - M_{i+1}}{T_i - T_{i+1}} \Delta H_i \tag{3}$$

The entropy change for $Pr_{0.6-x}Er_xSr_{0.4}MnO_3$ samples calculated as a function of temperature at various magnetic applied fields is given in Fig. 8. The maximum of the magnetic entropy change observed for $x = 0.0, 0.05, 0.1, 0.15$, and $x = 0.2$ samples at 2 T and 5 T are listed in Table 2. The large magnetocaloric effect in perovskite manganites could originate from the spin-lattice coupling in the magnetic ordering process [28, 29]. The strong coupling between spin and lattice has been shown by the observed lattice changes accompanying magnetic transitions in these manganites [30]. The lattice structure changes in the Mn–O bond distance as well as in the Mn–O–Mn bond angle, would in turn favor the spin ordering. Then a more abrupt variation of magnetization near the magnetic transition occurs and results in a large magnetic entropy change.

Relative cooling power or refrigerant capacity is a useful parameter, which is deciding the efficiency of magnetocaloric materials based on the magnetic entropy change [31, 32]. The estimated relative cooling power (RCP) is computed by RCP $= -\Delta S_M(T, H) \times \delta T_{FWHM}$ where δT_{FWHM} is the full width at half-maximum of the magnetic entropy change curve. This parameter corresponds to the amount of heat that can be transferred between the cold and hot parts of the refrigerator in one ideal thermodynamic cycle. The RCP allows an easy comparison of different magnetic materials for applications in magnetic refrigeration; hence, larger RCP values lead to better magnetocaloric materials. Our studied samples with modest values for the magnetic entropy change ΔS_M present RCP values of 223.3, 307.8, 294.46, 294.58 and 315.27 J/kg at 5 T for $x = 0.05, 0.1, 0.15$ and 0.2, respectively (see Table 2). These values are comparables, which confirm that the larger the δT_{FWHM}, the better the cooling capacity [33]. The RCP of our $Pr_{0.6-x}Er_xSr_{0.4}MnO_3$ ($0.0 \leq x \leq 0.2$) compounds are 54.46 %, 75.06 %, 71.81 %, 71.84 %, and 76.9 of RCP of Gd (410 J/kg) at 5 T [34]. These results are interesting
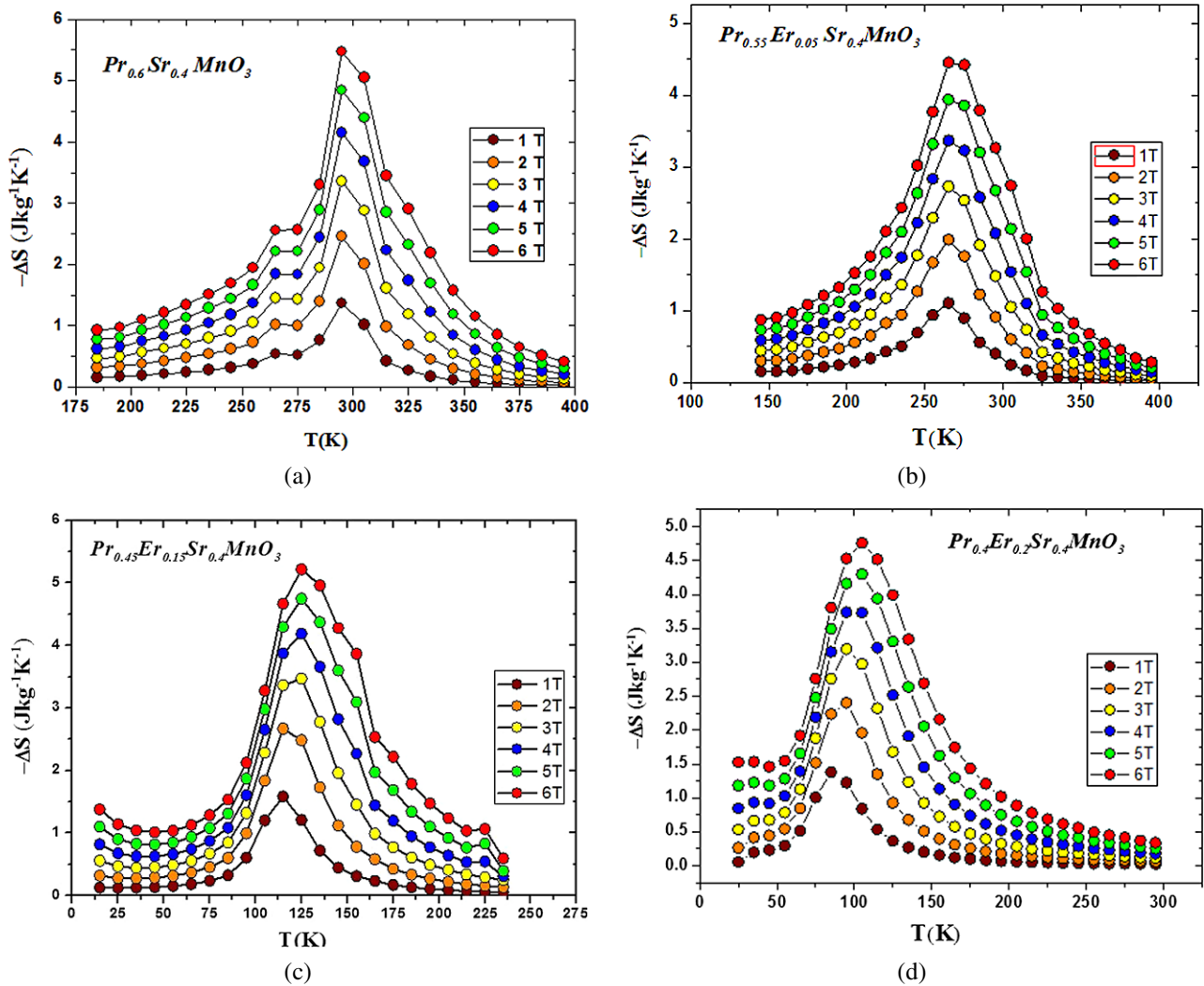
Fig. 8 Magnetic entropy change versus temperature at several magnetic applied field changes for the $Pr_{0.6-x}Er_xSr_{0.4}MnO_3$ samples: (**a**) $x = 0.0$, (**b**) $x = 0.05$, (**c**) $x = 0.15$, and (**d**) $x = 0.2$

enough, compared to those observed in other materials considered as good for applications in magnetic refrigerators, paving a way for investigations of materials useful for magnetic refrigeration.

6 Conclusion

Results on structural, magnetic, and magnetocaloric properties of Er doped manganites, $Pr_{0.6-x}Er_xSr_{0.4}MnO_3$ ($0.0 \leq x \leq 0.2$), have been presented and discussed. The powder samples were elaborated using the standard ceramic process. A structural analysis was carried out by means of X-ray diffraction and the Rietveld refinement method (all measurements were performed at room temperature). The samples were single-phase and crystallize in the orthorhombic structure with Pnma space group. Our compounds exhibit paramagnetic to ferromagnetic transition with decreasing tempera-

Table 2 Maximum entropy change and RCP values for all samples

x	$|\Delta S_M^{max}|$ (J kg^{-1} K^{-1})		RCP (J kg^{-1})	
	2 T	5 T	2 T	5 T
0.00	2.46	4.85	78.01	223.29
0.05	1.98	3.94	113.81	307.77
0.10	2.29	4.38	112.32	294.46
0.15	2.66	4.747	115.84	294.58
0.20	2.40	4.29	118.29	315.27
Gd	4 [35]	10.2 [34]	120 [35]	410 [34]

ture. The magnetic entropy change of $Pr_{0.6-x}Er_xSr_{0.4}MnO_3$ has been studied and ΔS_M is found to shift to higher values with increasing Er content. The variation of one single parameter, namely the Pr/Er ratio of the mixed-valence manganite series $Pr_{0.6-x}Er_xSr_{0.4}MnO_3$, has revealed a wide

range of interesting physical phenomena. It has also demonstrated a strategy for tailoring working substances for specific technological applications.

References

1. Dagotto, E., Hotta, T., Moreo, A.: Phys. Rep. **344**, 1 (2001)
2. Iliev, M.N., Abrashev, M.V., Popov, V.N., Hadjiev, V.G.: Phys. Rev. B **67**, 212301 (2003)
3. Zener, C.: Phys. Rev. **82**, 403 (1951)
4. Millis, A.J., Littlewood, P.B., Shraiman, B.J.: Phys. Rev. Lett. **74**, 5144 (1995)
5. Pollert, E., Jirák, Z., Hejtmánek, J., Strejc, A., Kužel, R., Hardy, V.: J. Magn. Magn. Mater. **246**, 290 (2002)
6. Wu, T., Mitchell, M.: Phys. Rev. B **69**, 100405 (2004)
7. Hebert, S., Maignan, A., Hardy, V., Martin, C., Hervieu, M., Raveau, B., Mahendiran, R., Schiffer, P.: Eur. Phys. J. B **29**, 419 (2002)
8. Mahandiran, R., Maignan, A., Hebert, S., Martin, C., Hervieu, M., Raveau, B., Mitchell, J.F., Schiffer, P.: Phys. Rev. Lett. **89**, 286602 (2002)
9. Panwar, N., Pandya, D.K., Rao, A., Wu, K.K., Kaurav, N., Kuo, Y.K., Agarwal, S.K.: Eur. Phys. J. B **65**, 179 (2008)
10. Boujelben, W., Ellouze, M., Cheikh-Rouhou, A., Pierre, J., Cai, Q., Yelon, W.B.: J. Alloys Compd. **334**, 1 (2002)
11. Rietveld, H.M.: J. Appl. Crystallogr. **2**, 65 (1969)
12. Rodriguez-Carvajal, J.: Physica B **192**, 55 (1993). For more details on the FULLPROF Suite of programs consult the site: http://www.ill.eu/sites/fullprof/
13. Shannon, R.D., Prewitt, C.T.: Acta Crystallogr., B Struct. Crystallogr. Cryst. Chem. **25**, 925 (1969)
14. Shannon, R.D., Prewitt, C.T.: Acta Crystallogr., B Struct. Crystallogr. Cryst. Chem. **26**, 1046 (1970)
15. Turpu, G.R., Gupta, A., Reddyo, K.R.: J. Phys. D, Appl. Phys. **42**, 145004 (2009)
16. M'nassri, R., Cheikhrouhou-Koubaa, W., Koubaa, M., Boudjada, N., Cheikhrouhou, A.: Solid State Commun. **151**, 1579 (2011)
17. Radaelli, P.G., Iannone, G., Marezio, M., Huang, H.Y., Cheong, S.W., Jorgensen, J.D., Argyriou, D.N.: Phys. Rev. B **56**, 8265 (1997)
18. Hwang, H.Y., Chong, S.W., Radaelli, P.G., Marezio, M., Batlogg, B.: Phys. Rev. Lett. **75**, 914 (1995)
19. Moutis, N., Panagiotopoulos, I., Pissas, M., Niarchos, D.: Phys. Rev. B **59**, 1129 (1999)
20. Wang, Z.M., Ni, G., Sang, H., Du, Y.W.: J. Magn. Magn. Mater. **234**, 213 (2001)
21. Ling, L., Fan, J., Pi, L., Tan, S., Zhan, Y.: Solid State Commun. **145**, 11 (2008)
22. Banerjee, B.K.: Phys. Lett. **12**, 16 (1964)
23. Deshmukh, A.V., Patil, S.I., Bhagat, S.M., Sagdeo, P.R., Choudhary, R.J., Phase, D.M.: J. Phys. D, Appl. Phys. **42**, 185410 (2009)
24. Dey, P., Nath, T.K.: Phys. Rev. B **73**, 214425 (2006)
25. Arrott, A., Noakes, J.E.: Phys. Rev. Lett. **19**, 786 (1967)
26. Morrish, A.H.: The Physical Principles of Magnetism. Wiley, New York (1965). Chap. 3
27. Foldeaki, M., Chahine, R., Bose, T.K.: J. Appl. Phys. **77**, 3528 (1995)
28. Phan, M.H., Yu, S.C., Hur, N.H., Yeong, Y.H.: J. Appl. Phys. **96**, 1154 (2004)
29. Radaelli, P.G., Cox, D.E., Marezio, M., Cheong, S.W., Schiffer, P.E., Ramirez, A.P.: Phys. Rev. Lett. **75**, 4488 (1995)
30. Guo, Z.B., Du, Y.W., Zhu, J.S., Huang, H., Ding, W.P., Feng, D.: Phys. Rev. Lett. **78**, 1142 (1997)
31. Pecharsky, V.K., Gschneidner, K.A., Tsokol, A.O.: Rep. Prog. Phys. **68**, 1479 (2005)
32. Gschneidner, K.A. Jr., Pecharsky, V.K.: Annu. Rev. Mater. Sci. **30**, 387 (2000)
33. Pecharsky, V.K., Gschneidner, K.A. Jr.: Phys. Rev. Lett. **78**, 4494 (1997)
34. Phan, M.H., Yu, S.C.: J. Magn. Magn. Mater. **306**, 325 (2007)
35. Tegus, O., Bruck, E., Buschow, K.H.J., de Boer, F.R.: Nature **415**, 150 (2002)